J. Phys.: Condens. Matter **23** (2011) 265502 (5pp) doi:10.1088/0953-8984/23/26/265502

Electronic structure of thermoelectric Zn–Sb

P H Michael Böttger[1], Spyros Diplas[2,3], Espen Flage-Larsen[1,3], Øystein Prytz[1] and Terje G Finstad[1]

[1] Department of Physics, University of Oslo, PO Box 1048 Blindern, 0316 Oslo, Norway
[2] Department of Chemistry, Centre of Material Science and Nanotechnology, University of Oslo, PO Box 1126 Blindern, 0318 Oslo, Norway
[3] SINTEF Materials and Chemistry, Forskningsveien 1, 0314 Oslo, Norway

E-mail: p.h.m.bottger@fys.uio.no

Received 11 April 2011, in final form 19 May 2011
Published 13 June 2011
Online at stacks.iop.org/JPhysCM/23/265502

Abstract
The electronic structures of the two main compounds of the binary zinc antimonides that are stable at room temperature, Zn_1Sb_1 and β-Zn_4Sb_3, were probed with x-ray photoelectron spectroscopy. Additionally, electron energy loss measurements and density functional theory calculations are presented. The compounds are found to share a very similar electronic structure. They both feature only small charge transfers and differ moderately in their screening potentials. These results are in line with recent theoretical works on the Zn–Sb system and are discussed in light of the reported thermoelectric performance of the materials.

1. Introduction

Thermoelectric conversion is the generation of electric power from temperature differences, and vice versa. Thermoelectric converters are made from pairs of n- and p-type heavily doped semiconductor legs being subject to temperature difference while being electrically connected in series. The applications range from Peltier elements for spot cooling and autonomous sensors to waste-heat recyclers and satellite power supplies. The efficiency of conversion is closely related to the dimensionless thermoelectric figure of merit zT:

$$zT = \frac{S^2\sigma}{\kappa}T. \quad (1)$$

Here S denotes the Seebeck coefficient, σ the electrical conductivity and κ the thermal conductivity of the material at a certain absolute temperature T. It is believed that the range of applications for thermoelectric conversion could be significantly increased if this figure of merit can be increased from the value $zT \approx 1$ of today's materials [1].

Zn–Sb alloys have been of interest for thermoelectric applications for decades [2] and the Zn–Sb phase was investigated early on. More recently, excellent thermoelectric properties ($zT \approx 1.3$ at 650 K) have been specifically reported for the β-Zn_4Sb_3 phase (referred to as Zn_4Sb_3 in this paper) due to an exceptionally low lattice thermal conductivity [3–5].

Engineering of materials to lower the lattice thermal conductivity, e.g. by introducing nanostructures, has been a promising route to improve on the figure of merit for different thermoelectric material systems [6, 7]. Because the thermal conductivity in Zn_4Sb_3 is already comparable to amorphous structures, reducing it further without affecting the electronic properties adversely does not seem promising. In this case, the power factor $S^2\sigma$ in the figure of merit (1) has to be improved. Analysis of the underlying electronic structure can help in this regard [8]. First-principles studies of the electronic structure of the Zn–Sb system have been published recently. Häussermann and Mikhaylushkin [9] describe crystals of ZnSb and Zn_4Sb_3 as 'electron-poor framework semiconductors' (EPFS). These EPFS are ascribed weakly polar sp-bonding and have a valence electron count lower than four. Qiu *et al* [10] present theoretical work on the Zn_4Sb_3 phase detailing the electronic structure and find their model of the structure describing a p-type semiconductor in accordance with the results of Snyder *et al* [4] with a band gap of 0.26 eV and hole concentration of 9×10^{19} cm^{-3}. In a recent work by Pomrehn *et al* [11] the formation energy of Zn_4Sb_3 is analysed and entropic stabilization of the phase is found at compositions that agree with the observed electronic properties.

Experimental work so far has focused on the thermoelectric properties of these materials. It is, however, difficult to extract information about the electronic structure directly from these types of measurements. Therefore the testing of the

theoretical electron structure and modelling is very indirect. More recently, x-ray photoelectron spectroscopy (XPS) has been used as a method for understanding specific problems in thermoelectrics, especially for testing density functional theory (DFT) results [12]. XPS can probe the density of states (DOS) and help determine the nature of chemical bonding and the electronic structure [13]. Electron energy loss spectroscopy (EELS) is an additional useful tool for determining charge transfers and interatomic bonding behaviour in alloys [14]. In this work we report on XPS and EELS studies of the electronic structure of ZnSb and Zn_4Sb_3 with the ultimate goal of better understanding the potential of these materials for thermoelectric applications as well as their electronic structure and properties.

2. Methods

2.1. Synthesis and characterization

To prepare the ZnSb samples stoichiometric amounts of Zn and Sb were sealed in an evacuated quartz glass vial. The sample was subsequently melted by heating in a gas flame and quenching in water. The ingot was then ground with an agate mortar, sealed in a glass vial again and annealed for five days at 510 °C. For Zn_4Sb_3 the samples were prepared similarly but melted at 700 °C for one day while being rocked. The sample was then also quenched in water, annealed for one day at 300 °C and quenched again. X-ray diffraction analysis (XRD) using Cu Kα radiation was employed to ensure that single phase material resulted. For reference measurements Zn (99.9999%, Sigma-Aldrich) and hydrothermally grown ZnO wafers (SPC Goodwill) were used.

2.2. XPS

XPS was performed on polished samples at room temperature using a Kratos AXIS Ultra DLD spectrometer and monochromatic Al Kα radiation ($h\nu = 1486.6$ eV). The survey spectra were acquired at 160 eV pass energy and the valence band spectra at 20 eV (ZnSb) or 5 eV (Zn_4Sb_3). The surface of the sample was analysed after Ar ion etching to minimize the C 1s and O 1s signals. The CasaXPS software package (www.casaxps.com) was employed for data processing.

2.3. EELS

Samples for EELS were prepared by mechanical grinding and standard ion-milling techniques. The EELS studies were performed using a post-column Gatan imaging filter fitted to a field emission JEOL 2010F transmission electron microscope (TEM) operated at 200 kV. The spectra were obtained with an energy resolution between 1.0 and 1.5 eV, as determined by the full width at half maximum of the zero-loss peak, and a spectrometer dispersion of 0.5 eV/channel. The spectra were corrected for channel-to-channel gain variations in the detector, and the dark current was subtracted. The experimental L edges were compared to spectra modelled using the RSMS (real-space multiple-scattering) code FEFF [15]. In these calculations, self-consistent muffin-tin potentials were obtained using Hedin–Lundqvist local-density approximation self-energies [16]. Potentials were calculated with and without a core hole in the 2p shell of the central atom. Spectra modelled in the presence of a core hole gave better correspondence with the experiments, and all spectra presented here were calculated with a core hole. Convergence tests were performed and the self-consistent field calculations were done on clusters of approximately 100 atoms, while for the multiple scattering calculations clusters of roughly 400 atoms were used.

2.4. DFT

Density functional calculations were performed in the Vienna *ab initio* simulation package (VASP) [17, 18] using the GGA-PBE (generalized gradient approximation of Perdew, Burke and Ernzerhof) [19] functional in the PAW (projector augmented wave) [20] formalism. An energy cut off of 550 eV and k-point density of $8 \times 8 \times 8$ were sufficient to converge the total energies within a few millielectronvolts. To simplify the calculations, the Zn_6Sb_5 structure was used as a model for the Zn_4Sb_3 [9]. Even though this model lacks the interstitials it still represent most of the Zn–Sb bonds further down in the valence band. Due to the lack of XPS resolution close to the band gap, we did not opt for a more complicated calculation with the interstitials, which in most cases modify the states with low binding energy. The structures were relaxed using experimental lattice parameters as input.

2.5. Auger parameter and Wagner plot

The Auger parameter α describes a measure of the chemical environment in XPS spectra. Using the shift between the Auger kinetic energy E_k of a core-level transition and the binding energy E_b of a corresponding core-level allows one to compare chemical compounds, eliminating the influence of different energy referencing in the process:

$$\alpha = E_b + E_k. \tag{2}$$

Wagner found that the difference $\Delta\alpha$ in this 'final state' Auger parameter between two compounds yields the difference in relaxation energy R [21]. This relaxation energy can be understood as the response of the local electronic structure to the creation of holes and is connected to the screening potential and charge transfer via

$$\Delta\alpha = \Delta\left[q\frac{\mathrm{d}k}{\mathrm{d}N} + \left(k - 2\frac{\mathrm{d}k}{\mathrm{d}N}\right)\frac{\mathrm{d}q}{\mathrm{d}N} + \frac{\mathrm{d}U}{\mathrm{d}N}\right]. \tag{3}$$

The three terms stand for the shrinkage of the occupied valence orbitals when a core electron is removed, the transferred screening from the surroundings, and the effect of polarization by the core hole, respectively. Additionally, an initial state Auger parameter β can be defined by

$$\beta = E_k + 3E_b \tag{4}$$

and shifts in this parameter value can be used to quantify changes in the initial state atomic potential between two environments [22]. It is, however, not as strong as α in its

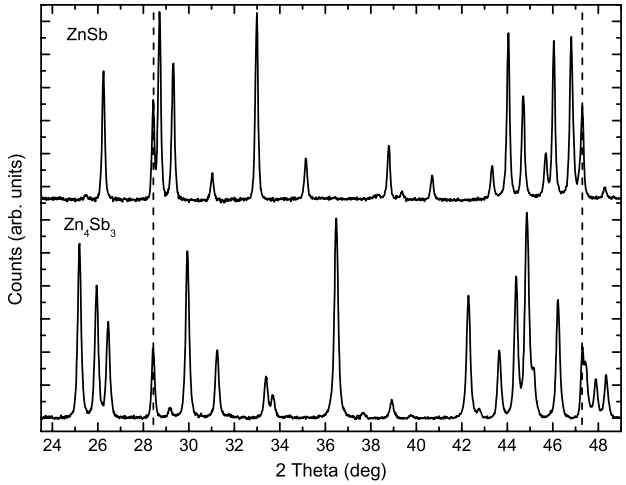

Figure 1. Detail of the XRD scan of ZnSb (top) and Zn_4Sb_3 (bottom). Dashed lines indicate the admixed Si standard.

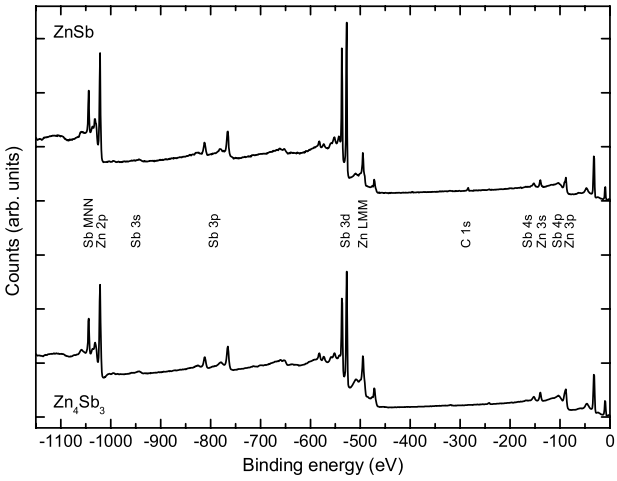

Figure 2. XPS survey scan of ZnSb (top) and Zn_4Sb_3 (bottom). Selected identifying features are labelled.

Table 1. XPS peak positions used for Auger parameter determination. Zn $L_3M_{45}M_{45}$ is given as a kinetic energy.

Sample	Zn $L_3M_{45}M_{45}$ (eV)	Zn $2p_{3/2}$ (eV)	α (eV)
ZnSb	991.8	1021.3	2013.1
Zn_4Sb_3	991.54	1021.69	2013.23
Zn	992.25	1021.4	2013.65
ZnO	988.29	1022.15	2010.44

predictive power since it relies on a simple electrostatic model for the outer electron shells and is not immune to energy referencing effects. In order to compare and classify different chemical environments, Moretti [13], in a so-called Wagner plot, plotted E_k values of the Zn $L_3M_{45}M_{45}$ Auger line over E_b values of the Zn $2p_{3/2}$ peak for many different Zn compounds. In this plot constant α and β parameters are lines of different slopes. All Zn compounds surveyed fitted into the window between the border lines spanned by the Auger parameters of metallic Zn and ionic ZnF_2.

3. Results

The observed x-ray patterns (figure 1) show a single phase material. The crystal structure of ZnSb is orthorhombic (space group 61; $Pbca$) and Zn_4Sb_3 is rhombohedral (space group 167; $R\bar{3}c$). No indication of metallic phases of Zn or Sb could be found in the patterns.

The XPS survey scans shown in figure 2 are indistinguishable except for the adventitious C 1s peak. This stems from surface or chamber contamination and is being used for energy referencing with a fixed value of 284.8 eV. The labelling of the peaks illustrates that only the Zn LMM Auger event can be used for the Auger parameter in the energy range open to Al Kα radiation. We use the line with the strongest signal, which is Zn $L_3M_{45}M_{45}$.

The difference in the Zn 2p-$L_3M_{45}M_{45}$ Auger parameter between the two Zn–Sb compounds seen in table 1 is very small and within the instrumental error ($\approx$0.1 eV per peak position). The values of their Auger parameters are much

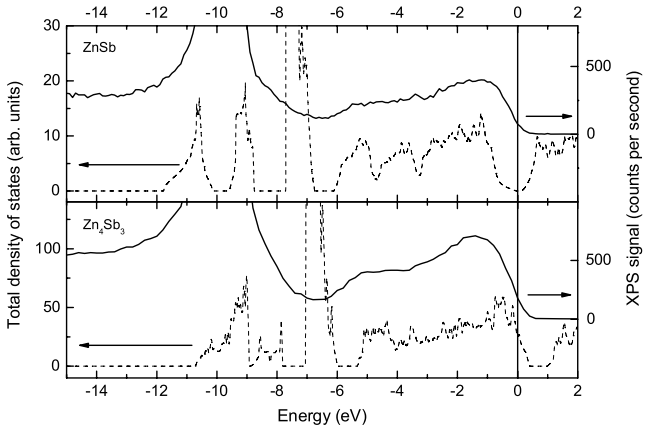

Figure 3. Valence band spectrum of ZnSb and Zn_4Sb_3 with the total integrated DFT DOS results. The Fermi level is drawn at 0 eV.

closer to the metallic bound Zn than to the ionic ZnO. The details of the relative peak positions in these samples will be discussed with the Wagner plot in section 4.

When looking at the valence band spectrum of the compounds in figure 3, the features are also very similar. The DFT results are off for the Zn 3d peak; these were reported earlier for Zn compounds and are due to delocalization errors of the d states when using standard functionals [12]. The calculated valence states from the Fermi level down to −5 eV follow the experimentally found distribution but are off in their estimate of the carrier concentration (and thus also the position of the chemical potential). This is a common occurrence in DFT calculations but has been demonstrated in the case of Zn_4Sb_3 to be alleviated by a more complex structural description including vacancies and interstitials [9].

The EELS spectra of the Zn $L_{2,3}$ edge and the overhead fine structure of the two Zn–Sb compounds together with one for pure Zn are shown in figure 4. As the fine structure above the edge is determined by the same kind of process as in XPS, that is electron ejection followed by recombination, the EELS spectra are also found to be virtually identical. They

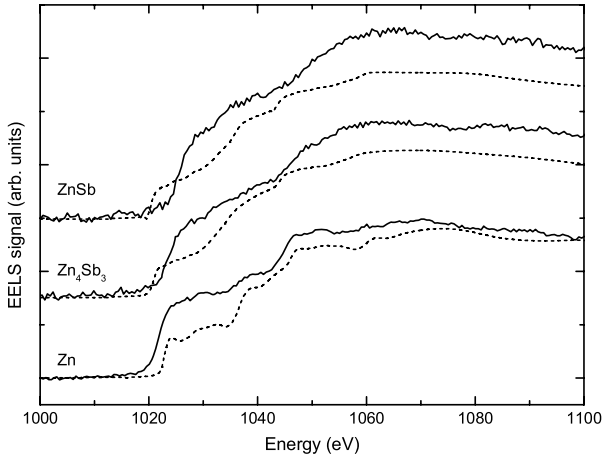

Figure 4. EELS spectra (solid lines) and FEFF results (dotted lines) for the Zn $L_{2,3}$ line in the ZnSb, Zn_4Sb_3 and in pure Zn.

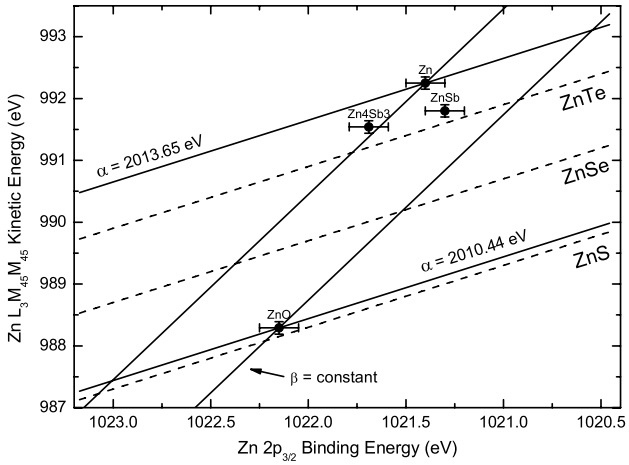

Figure 5. Wagner plot for the Zn–Sb compounds set between metallic Zn and strongly polar ZnO. Additional lines are from the NIST XPS database [25].

Table 2. FEFF orbital occupancy.

Orbital	Zn	Sb		Zn_6Sb_5	
Zn s	1			1.052	
Zn p	0.973			0.963	
Zn d	10.028			10.098	
				Sb(1)	Sb(2)
Sb s		1.862		1.783	1.784
Sb p		2.797		2.895	2.739
Sb d		10.341		10.249	10.250
Sum	12.001	15.000	12.113	14.926	14.773

are, however, very different from metallic Zn showing fewer features in the fine structure region. The FEFF calculations show qualitatively the same softening of the fine structure features. They can be used to predict charge transfer as shown in table 2 for the Zn_6Sb_5 model system. The amount of charge transfer, however, is very small, about $0.1e$ moving from Sb to Zn. The softening can, in a most general way, be attributed to a loss in symmetry, or coordination, as the number of available final states increases [23].

4. Discussion

While the crystal symmetries are different, the close range binding structure, or coordination, of the two Zn–Sb phases is quite similar. Häussermann and Mikhaylushkin [9] describe them both as composed of planar rhomboids, consisting of two Zn and Sb atoms each ('Zn_2Sb_2'). In that picture they are meant to be arranged as separate rings in ZnSb while they comprise one-dimensional chains in Zn_4Sb_3, sharing one Sb atom position. This similarity is reflected in our results.

A Wagner plot for the Zn 2p-$L_3M_{45}M_{45}$ Auger parameter is presented in figure 5. It shows the proximity of the Zn–Sb compounds to metallic Zn in comparison to ZnO indicating a weakly ionic bonding. The Auger parameter is not appreciably shifted between ZnSb and Zn_4Sb_3, suggesting a similar amount of charge transfer and polarization energy. The closeness to metallic Zn allows for a rough estimate of the charge transfer. If one assumes metallic bonding, equation (3) can be simplified with $\mathrm{d}q/\mathrm{d}N = 1$ because exactly one electron is moving from the conduction band to any core hole and $\mathrm{d}U/\mathrm{d}N = 0$, because metallic screening does not allow for local polarization. With computational values for $\mathrm{d}k/\mathrm{d}N$ for Zn, estimated from the work of Gregory *et al* [24] as about -4 eV, the Auger shift $\Delta\alpha$ of roughly 0.5 eV between Zn and ZnSb amounts to a charge transfer in Zn of $0.13e$. This is in line with the results from FEFF calculations presented in table 2.

Strong polar bonding is unwelcome in thermoelectric materials because of the mobility decrease that comes with polar scattering [26]. The Zn–Sb compounds have a negligible charge transfer so the rather low mobility of Zn_4Sb_3 [3] cannot be attributed mainly to the difference in electronegativity. The unique very big unit cell structure of the compound that includes vacancies and interstitials [4] and other features like internal strains may contribute to a low mobility. However, the largest cause might be the fact that the conducting electron bands have a rather large effective mass (e.g. flat defect bands for the interstitials) and thus yield low mobility. The vast numbers of states in the Zn_4Sb_3 compensate for the low mobility by a large carrier concentration such that the electronic conductivity is still large enough to obtain high values for the figure of merit.

5. Conclusions

The electronic structure of the two main phases in the binary Zn–Sb system, ZnSb and Zn_4Sb_3, are found to be very similar. This is ascribed to their similar close range atomic ordering where rhomboids of 'Zn_2Sb_2' form the basic element. They both show only weak polar bonding with very small charge transfers. From the very similar coarse electronic structure between the two compounds one could also expect similarities in the details of the structure close to the Fermi level which has the most influence on the thermoelectric properties. However, that remains undetermined with the current resolution and precision in theoretical calculation and experimental techniques.

Acknowledgments

Funding from the Norwegian Research Council is gratefully acknowledged. The authors would also like to thank Martin F Sunding for carrying out some of the XPS measurements, the thermoelectrics group at Caltech for supplying the Zn_4Sb_3 sample and Ole Bjørn Karlsen for support in sample preparation.

References

[1] DiSalvo F J 1999 Thermoelectric cooling and power generation *Science* **285** 703–6

[2] Vedernikov M V and Iordanishvili E K 1998 A F Ioffe and origin of modern semiconductor thermoelectric energy conversion *ICT 98: 17th Int. Conf. on Thermoelectrics* vol 1, pp 37–42

[3] Caillat T, Fleurial J-P and Borshchevsky A 1997 Preparation and thermoelectric properties of semiconducting Zn_4Sb_3 *J. Phys. Chem. Solids* **58** 1119–25

[4] Snyder G J, Christensen M, Nishibori E, Caillat T and Iversen B B 2004 Disordered zinc in Zn_4Sb_3 with phonon-glass and electron-crystal thermoelectric properties *Nature Mater.* **3** 458–63

[5] Toberer E S, Rauwel P, Gariel S, Taftø J and Snyder J G 2010 Composition and the thermoelectric performance of β-Zn_4Sb_3 *J. Mater. Chem.* **20** 9877–85

[6] Poudel B *et al* 2008 High-thermoelectric performance of nanostructured bismuth antimony telluride bulk alloys *Science* **320** 634–8

[7] Biswas K, He J, Zhang Q, Wang G, Uher C, Dravid V P and Kanatzidis M G 2011 Strained endotaxial nanostructures with high thermoelectric figure of merit *Nature Chem.* **3** 160–6

[8] Minnich A J, Dresselhaus M S, Ren Z F and Chen G 2009 Bulk nanostructured thermoelectric materials: current research and future prospects *Energy Environ. Sci.* **2** 466–79

[9] Häussermann U and Mikhaylushkin A S 2010 Electron-poor antimonides: complex framework structures with narrow band gaps and low thermal conductivity *Dalton Trans.* **39** 1036–45

[10] Qiu A N, Zhang L T and Wu J S 2010 Crystal structure, electronic structure, and thermoelectric properties of β-Zn_4Sb_3 from first principles *Phys. Rev.* B **81** 035203

[11] Pomrehn G S, Toberer E S, Snyder G J and van de Walle A 2011 Entropic stabilization and retrograde solubility in Zn_4Sb_3 *Phys. Rev.* B **83** 094106

[12] Flage-Larsen E, Diplas S, Prytz Ø, Toberer E S and May A F 2010 Valence band study of thermoelectric Zintl-phase $SrZn_2Sb_2$ and $YbZn_2Sb_2$: x-ray photoelectron spectroscopy and density functional theory *Phys. Rev.* B **81** 205204

[13] Moretti G 1998 Auger parameter and Wagner plot in the characterization of chemical states by x-ray photoelectron spectroscopy: a review *J. Electron Spectrosc. Relat. Phenom.* **95** 95–144

[14] Muller D A, Singh D J and Silcox J 1998 Connections between the electron-energy-loss spectra, the local electronic structure, and the physical properties of a material: a study of nickel aluminum alloys *Phys. Rev.* B **57** 8181–202

[15] Ankudinov A L, Ravel B, Rehr J J and Conradson S D 1998 Real-space multiple-scattering calculation and interpretation of x-ray-absorption near-edge structure *Phys. Rev.* B **58** 7565

[16] Hedin L and Lundqvist B I 1971 Explicit local exchange–correlation potentials *J. Phys. C: Solid State Phys.* **4** 2064

[17] Kresse G and Hafner J 1993 *Ab initio* molecular dynamics for liquid metals *Phys. Rev.* B **47** 558

[18] Kresse G and Furthmüller J 1996 Efficiency of *ab initio* total energy calculations for metals and semiconductors using a plane-wave basis set *Comput. Mater. Sci.* **6** 15–50

[19] Perdew J P, Burke K and Ernzerhof M 1996 Generalized gradient approximation made simple *Phys. Rev. Lett.* **77** 3865–8

[20] Kresse G and Joubert D 1999 From ultrasoft pseudopotentials to the projector augmented-wave method *Phys. Rev.* B **59** 1758–75

[21] Wagner C D 1975 Chemical shifts of Auger lines, and the Auger parameter *Faraday Discuss.* **60** 291–300

[22] Evans J A, Laine A D, Weightman P, Matthew J A D, Woolf D A, Westwood D I and Williams R H 1992 Charge transfer across the As/Si(100) interface *Phys. Rev.* B **46** 1513–20

[23] Taftø J and Zhu J 1982 Electron energy loss near edge structure (ELNES), a potential technique in the studies of local atomic arrangements *Ultramicroscopy* **9** 349–54

[24] Gregory D A C, Laine A D, Fowles P S, Takahashi A and Weightman P 1993 Atomic structure calculations for the analysis of Auger parameters of elements K to Kr *J. Phys.: Condens. Matter* **5** 3843

[25] *NIST X-Ray Photoelectron Spectroscopy Database* 2003 (Gaithersburg: National Institute of Standards and Technology) http://srdata.nist.gov/xps/

[26] Slack G A 1995 *New Materials and Performance Limits for Thermoelectric Cooling* 1st edn *CRC Handbook of Thermoelectrics* (Boca Raton, FL: CRC Press) chapter 34, pp 407–40